MULTI-SPIKE SOLUTIONS TO THE ONE-DIMENSIONAL SUBCRITICAL FRACTIONAL SCHNAKENBERG SYSTEM

DANIEL GOMEZ, JUN-CHENG WEI, AND ZHANGYU YANG

Abstract. Singularly perturbed reaction-diffusion systems such as the Gierer-Meinhardt, Schankenberg, and Gray-Scott models are known to exhibit localized multi-spike solutions in which one of the species concentrates on a discrete collection of well-separated points. A recent focus has been the extension of the analysis, both rigorous and formal, of such localized solutions to the case where classical diffusion is replaced by anomalous diffusion exhibiting Lévy flights. Mathematically, such systems replace the classical Laplacian with the fractional Laplacian $(-\Delta)^s$ where s is the fractional order. In this paper we consider the formal analysis of multi-spike solutions to the fractional Schnakenberg system with periodic boundary conditions when the fractional order of the activator satisfies $1/4 < s_1 < 1$ and that of the substrate satisfies $1/2 < s_2 < 1$. Using the method of matched asymptotic expansions we derive a nonlinear algebraic system that determines the structure of equilibrium solutions, a nonlocal eigenvalue problem that determines its linear stability over a fast, $O(1)$, timescale, as well as a system of ordinary differential equations that determine the dynamics of multi-spike solutions over a slow, $O(\varepsilon^{-2})$, timescale. We explicitly construct symmetric multi-spike solutions and derive stability criteria for instabilities arising over both fast and slow timescales. One of the key findings in this paper is that the slow timescale instability thresholds are, barring symmetry considerations, less degenerate than in the classical $s_2 = 1$ case. In addition we numerically calculate bifurcation diagrams that show how asymmetric multi-spike solutions branch out from symmetric ones at distinct points for solutions with five or more spikes.

Keywords: Schnakenberg system, fractional Laplacian, Lévy flights, localized solutions, singular perturbation, matched asymptotic expansions.

1. Introduction

Singularly perturbed *activator-inhibitor* or *activator-substrate* reaction-diffusion systems in which the activator's diffusivity $\varepsilon^2 \ll 1$ is asymptotically small, are known to exhibit localized spike solutions. Such solutions are characterized by an activator that is localized within $O(\varepsilon)$ neighbourhoods of a discrete set of points and an inhibitor or substrate that is globally variable. This asymptotically large separation between characteristic length scales has made such models particularly amenable to both rigorous and formal analysis. In particular, it is possible in these systems to obtain detailed properties of equilibrium solutions arising far-from equilibrium, i.e. well beyond the onset of linear (Turing) instabilities [21, 29]. Prototypical examples of such singularly perturbed reaction diffusion systems include the Gierer-Meinhardt, Gray-Scott, Brusselator and Schnakenberg systems, the latter of which will be the focus of this paper. The method of matched asymptotic expansions has been remarkably successful in probing the structure, linear stability, and slow-dynamics of localized solutions in each of these models starting with pioneering work of Iron, Ward, and Wei in 2001 on the one-dimensional Gierer-Meinhardt system [12]. Subsequent studies have considered properties of localized solutions in other contexts including, but not limited to, higher-dimensional domains [14, 25, 7], curved surfaces [22], and bulk-surface coupled systems [6]. Additionally, rigorous methods based on Lyapunov Schmidt reductions and spectral estimates have been used to rigorously establish the existence and stability properties of localized solutions for the Gierer-Meinhardt and other singularly perturbed reaction-diffusion systems [28, 29, 24].

A growing body of literature has studied localized spike solutions to the one-dimensional *fractional* singularly perturbed Gierer-Meinhardt system in which classical diffusion is replaced with anomalous

diffusion exhibiting Lévy flights. Mathematically, the introduction of such an anomalous diffusion amounts to replacing the classical (local) Laplacian $(-\Delta)$ with the (nonlocal) fractional Laplacian $(-\Delta)^s$ where s is referred to as the fractional order and which we define below. Using the method of matched asymptotic expansion, Y. Nec first investigated the effects on the structure and linear stability of localized spike solutions when Lévy flights are introduced into the activator equation [20]. This was followed by Wei and Yang who rigorously proved the existence of multi-spike solutions in the fractional Gierer-Meinhardt system on the real line when the fractional order of both the inhibitor and activator is $s \in [1/2, 1)$ [30]. More recently, both formal and rigorous methods have been used to investigate multi-spike solutions in bounded domains where the fractional order of the activator is $s \in (1/4, 1)$ while that of the inhibitor is $s \in [1/2, 1)$ [8], $s = 1/2$ [17], and $s \in (0, 1/2)$ [5]. As highlighted in [5], one can draw analogies between the fractional Gierer-Meinhardt system in $\mathbb{R}^1$ with the classical Gierer-Meinhardt system in $\mathbb{R}^1$, $\mathbb{R}^2$, and $\mathbb{R}^3$, with this connection being closely related to the singular behaviour of the fractional free-space Green's function. Specifically, when the fractional order is $s < 1/2$ (supercritical case) the free-space Green's function has an algebraic singularity, when $s = 1/2$ (critical case) it has a logarithmic singularity, and when $s > 1/2$ (subcritical case) is it non-singular (though its first derivative is discontinuous). The behaviour in each of these regimes respectively parallels that of the classical free-space Green's function in $\mathbb{R}^3$, $\mathbb{R}^2$, and $\mathbb{R}^1$.

Interest in fractional reaction-diffusion systems, or anomalous diffusion systems more generally, is not limited to localized solutions in the singularly perturbed case. Indeed, anomalous systems are not only theoretically interesting in their own right but also have wide applicability in the natural sciences [18, 15, 1]. In the pattern formation literature, several studies have considered both the linear (Turing) stability analysis [9, 4] and the weakly-nonlinear analysis [31, 13] of anomalous counterparts to classical reaction-diffusion systems, while solitons and other localized solutions have likewise been numerically and theoretically studied in the fractional nonlinear Schrödinger equation [16]. In addition to studying specific solutions of fractional systems, the past few years have also seen the development of a growing toolbox for both the numerical simulation of fractional systems [10, 19] as well as their numerical continuation [3]. Within this larger context, the detailed asymptotic analysis of localized solutions in singularly perturbed reaction-diffusion systems offers both an impetus for rigorous studies while also providing markers for what kind of behaviour such systems may exhibit.

In this paper we consider the structure and linear stability of spike solutions to the fractional Schnakenberg reaction-diffusion system given by

$$\begin{cases} u_t + \varepsilon^{2s_1}(-\Delta)^{s_1} u + u - u^2 v = 0, & -1 < x < 1, \qquad (1.1a) \\ \varepsilon v_t + D(-\Delta)^{s_2} v - 2^{-1} + \varepsilon^{-1} A u^2 v = 0, & -1 < x < 1, \qquad (1.1b) \\ u(x+2) = u(x), \qquad v(x+2) = v(x), & x \in \mathbb{R}. \qquad (1.1c) \end{cases}$$

Here we assume that $\varepsilon \ll 1$ is asymptotically small, while $D = O(1)$ and $A = O(1)$ with respect to $\varepsilon \ll 1$. In addition we assume that the fractional orders satisfy

$$1/4 < s_1 < 1, \qquad 1/2 < s_2 < 1. \qquad (1.2)$$

The fractional Laplacian appearing in (1.1) is defined by

$$(-\Delta)^s \varphi(x) = C_s \int_{-\infty}^{\infty} \frac{\varphi(x) - \varphi(\bar{x})}{|x - \bar{x}|^{1+2s}} d\bar{x}, \qquad C_s = \frac{2^{2s} s \Gamma(s + 2^{-1})}{\sqrt{\pi}\Gamma(1 - s)}, \qquad (1.3)$$

where $\Gamma(z)$ is the Gamma function and which, in light of the periodic boundary conditions in (1.1), simplifies to

$$(-\Delta)^s\varphi(x) = C_s\int_{-1}^{1} K_s(x-\bar{x})(\varphi(x)-\varphi(\bar{x}))d\bar{x}, \tag{1.4a}$$

$$K_s(z) := \frac{1}{|z|^{1+2s}} + \sum_{j=1}^{\infty}\left(\frac{1}{|z+2j|^{1+2s}} + \frac{1}{|z+2j|^{1-2s}}\right). \tag{1.4b}$$

Finally, we remark that an equivalent way to define the fractional Laplacian is in terms of its spectral decomposition which takes the form

$$(-\Delta)^s\varphi = \sum_{n=1}^{\infty}(n\pi)^{2s}\left(\cos(n\pi x)\int_{-1}^{1}\cos(n\pi\bar{x})\varphi(\bar{x})d\bar{x} + \sin(n\pi x)\int_{-1}^{1}\sin(n\pi\bar{x})\varphi(\bar{x})d\bar{x}\right), \tag{1.5}$$

with this final form being particularly useful when computing the relevant fractional Green's function.

The remainder of the paper is organized as follows. First, in §2 we use the method of matched asymptotic expansions to derive a nonlinear algebraic system (NAS) with which N-spike quasi-equilibrium solutions can be constructed. Particular attention is paid to the case of symmetric N-spike solutions for which the NAS can be solved explicitly. We follow this with a detailed asymptotic analysis of the linear stability of symmetric N-spike solutions. First, linear stability with respect to the large eigenvalues is considered in §3 by deriving a nonlocal eigenvalue problem (NLEP). This is followed in §4 by a derivation of a system of ordinary-differential-equations (ODEs) dictating the slow-dynamics of N-spike solutions. The linearization of this ODE system about the symmetric N-spike solution configuration then yields the linear stability of these solutions with respect to the small eigenvalues. In §5 we use the numerical continuation software PyDSTool [2] to construct bifurcation diagrams. These diagrams illustrate how asymmetric solutions branch from symmetric solutions at the small eigenvalue stability thresholds. In §6 we briefly outline the calculation of large and small eigenvalue thresholds for the Gierer-Meinhardt system to illustrate similarities with the Schnakenberg system. In §7 we briefly outline the numerical method used to simulate the full system (1.1) to validate the asymptotics and include some plots showing the dynamics of an N-spike solution for $N = 4, 5$. Finally, we summarize our results and suggest some directions for future research in §8.

2. Asymptotic Construction of Quasi-Equilibrium Solutions

The equilibrium problem is

$$\begin{cases} \varepsilon^{2s_1}(-\Delta)^{s_1}u + u - u^2v = 0, & -1 < x < 1, \quad (2.1a)\\ D(-\Delta)^{s_2}v - \frac{1}{2} + \frac{1}{\varepsilon}Au^2v = 0, & -1 < x < 1, \quad (2.1b)\\ u(x+2) = u, \qquad v(x+2) = v(x). & (2.1c) \end{cases}$$

in this section we will use the method of matched asymptotic expansions to construct solutions to (2.1). Specifically, we will construct N-spike solutions in which $u(x)$ concentrates at N well-separated points $-1 < x_1 < \cdots < x_N < 1$ in the sense that

$$|x_i - x_j| \gg \varepsilon \quad \text{for all } i \neq j, \qquad 2 + x_1 - x_N \gg \varepsilon. \tag{2.2}$$

The second condition above ensures x_1 and x_N are well-separated given that we are considering periodic boundary conditions.

We begin by introducing rescaled variables $u(x_i+\varepsilon y)\sim U_i(y)$ and $v(x_i+\varepsilon y)\sim V_i(y)$ to get the inner problem

$$\begin{cases}(-\Delta)^{s_1}U_i+U_i-U_i^2V_i=0, & -\frac{1+x_i}{\varepsilon}<y<\frac{1-x_i}{\varepsilon}, \quad (2.3a)\\ D(-\Delta)^{s_2}V_i-\frac{\varepsilon^{2s_2}}{2}+\varepsilon^{2s_2-1}AU_i^2V_i=0, & -\frac{1+x_i}{\varepsilon}<y<\frac{1-x_i}{\varepsilon}, \quad (2.3b)\end{cases}$$

where $U_i\to 0$ as $|y|\to\infty$ and the far-field behaviour of V_i is determined by the limiting behaviour of the outer problem as $x\to x_i$. Observe that $V_i(y)\sim \xi_i^{-1}+$ h.o.t where ξ_i is a constant that remains to be found and h.o.t denotes higher-order-terms. In terms of the undetermined constant ξ_i we write $U_i(y)\sim \xi_i w(y)+$h.o.t where $w(y)$ is the *fractional homoclinic* satisfying (see Proposition 4.1 in [30])

$$(-\Delta)^{s_1}w+w-w^2=0,\quad -\infty<y<\infty;\qquad w(y)\sim\frac{\mathfrak{b}_{s_1}}{|y|^{1+s_1}}\left(1+o(1)\right),\quad |y|\to\infty, \tag{2.4}$$

where $\mathfrak{b}_{s_1}$ is a constant that must in general be calculated numerically. Note that when $s_1=1/2$ we can explicitly calculate $w(y)=2/(1+y^2)$.

We now consider the outer problem by first making note of the distributional limit

$$\frac{1}{\varepsilon}u^2\longrightarrow\omega\sum_{j=1}^N\xi_j^2\delta(x-x_j),\qquad \omega:=\int_{-\infty}^{\infty}w(y)^2dy, \tag{2.5}$$

in terms of which we find that the outer problem for v is

$$D(-\Delta)^{s_2}v-\frac{1}{2}+A\omega\sum_{j=1}^N\xi_j\delta(x-x_j)=0,\quad x\in(-1,1)\setminus\{x_1,...,x_N\}. \tag{2.6}$$

Note that for $s_1=1/2$ we have $\omega=2\pi$. Furthermore, from the above equation we deduce the *solvability condition*

$$\sum_{j=1}^N\xi_j=\frac{1}{A\omega}. \tag{2.7}$$

Provided the solvability condition is satisfied we obtain the outer solution

$$v(x)\sim\frac{A\omega}{D}\sum_{j=1}^N\xi_jG(x-x_j)+\chi,\qquad x\in(-1,1)\setminus\{x_1,...,x_N\}, \tag{2.8}$$

where χ is an undetermined constant and $G(x)$ is the fractional Green's function satisfying

$$(-\Delta)^{s_2}G(x)-\frac{1}{2}+\delta(x)=0,\quad -1<x<1;\quad G(x+2)=G(x);\quad \int_{-1}^1G(x)dx=0. \tag{2.9}$$

Using the spectral definition it is straightforward to calculate

$$G(x)=-\sum_{n=1}^{\infty}\frac{\cos n\pi x}{(n\pi)^{2s_2}}, \tag{2.10}$$

which with a little more work can be rewritten as

$$G(x)=-\mathfrak{a}_{s_2}|x|^{2s_2-1}+R(x), \tag{2.11}$$

where

$$\mathfrak{a}_{s_2}:=-\frac{2s_2\Gamma(-2s_2)\sin(\pi s_2)}{\pi}. \tag{2.12}$$

and $R(x)$ is the regular part given by (A.3) in Appendix A. Evaluating the outer solution (2.8) at x_i and comparing this with the leading order behaviour of $V_i(y)$ as $|y| \to \infty$ yields the matching condition

$$\xi_i^{-1} = \frac{A\omega}{D} \sum_{j=1}^{N} \xi_j G(x_i - x_j) + \chi.$$

Multiplying both sides by ξ_i, summing over all $i = 1, ..., N$, and using the solvability condition (2.7), we can solve for

$$\chi = NA\omega - (A\omega)^2 D^{-1} \sum_{i,j=1}^{N} \xi_i \xi_j G(x_i - x_j).$$

To more succinctly summarize our results we define the $N \times N$ matrix $\mathcal{G}$ with entries

$$\mathcal{G}_{ij} := G(x_i - x_j), \qquad i, j = 1, ..., N, \tag{2.13}$$

as well as the N-dimensional vectors $\boldsymbol{\xi}$, $\boldsymbol{\xi}^\alpha$, and $\boldsymbol{e}_N$ respectively given by

$$\boldsymbol{\xi} := (\xi_1, ..., \xi_N)^T, \quad \boldsymbol{\xi}^\alpha := (\xi_1^\alpha, ..., \xi_N^\alpha)^T, \quad \boldsymbol{e}_N = (1, ..., 1)^T, \tag{2.14}$$

where $\alpha \in \mathbb{R}$ is arbitrary. The following proposition then summarizes the the above asymptotic construction.

Proposition 2.1. *Let w be the fractional homoclinic solution to(2.4), $\omega := \int_{-\infty}^{\infty} w^2 dy$, and $G(x)$ be the fractional Green's function satisfying (2.9). Given N well-separated points $-1 < x_1 < ... < x_N < 1$ in the sense of (2.2), the equilibrium system (2.1) admits the following asymptotic solution for $\varepsilon \ll 1$*

$$u_e(x) \sim \sum_{j=1}^{N} \xi_j w\left(\frac{x - x_i}{\varepsilon}\right), \qquad v_e(x) \sim \frac{A\omega}{D} \sum_{j=1}^{N} \xi_j G(x - x_j) + \chi, \tag{2.15a}$$

where $\chi = NA\omega - (A\omega)^2 D^{-1} \boldsymbol{\xi}^T \mathcal{G} \boldsymbol{\xi}$ and $\boldsymbol{\xi}$ is determined by solving the nonlinear-algebraic-system (NAS)

$$\boldsymbol{\xi}^{-1} = \frac{A\omega}{D} \mathcal{G}\boldsymbol{\xi} + \chi \boldsymbol{e}_N. \tag{2.15b}$$

2.1. **Symmetric N-Spike Solutions.** Symmetric N-spike solutions are characterized by having the same spike *heights*, i.e. for which $\boldsymbol{\xi} = \xi_c \boldsymbol{e}_N$. From the solvability condition (2.7) it is immediately clear that in such a case

$$\xi_c = \frac{1}{NA\omega}. \tag{2.16}$$

However, in light of the NAS (2.15b) we see that arbitrary spike configurations $-1 < x_1 < ... < x_N < 1$ will in general not yield such a solution. Indeed, for $\boldsymbol{\xi} = \xi_c \boldsymbol{e}_N$ to solve the (2.15b) we require that $-1 < x_1 < ... < x_N < 1$ be chosen in such a way that $\boldsymbol{e}_N$ is an eigenvector of $\mathcal{G}$. For the remainder of the paper, when we refer to symmetric solutions we will be assuming that the spike configuration is given by

$$x_j = -1 + \frac{2j - 1}{N}, \qquad j = 1, ..., N. \tag{2.17a}$$

In this case the matrix $\mathcal{G}$ is circulant (see Appendix B) and we can readily calculate

$$\mathcal{G}\boldsymbol{e}_N = \mu_N \boldsymbol{e}_N, \qquad \mu_N = \sum_{k=0}^{N-1} G(2k/N). \tag{2.17b}$$

3. Linear Stability of Symmetric N-Spike Solutions: Large Eigenvalues

Singularly perturbed reaction diffusion systems are known to exhibit linear instabilities over two distinguished timescales and these correspond to *large* and *small* eigenvalues of the linearized system. In this section we consider the linear stability of the quasi-equilibrium solutions from Proposition 2.1 with respect to the *large* eigenvalues. We let $\lambda = O(1)$ and substitute $u = u_e + e^{\lambda t}\phi$ and $v = v_e + e^{\lambda t}\psi$ into (1.1), retaining only linear terms in ϕ and ψ to obtain the linearized stability problem

$$\begin{cases} \varepsilon^{2s_1}(-\Delta)^{s_1}\phi + \phi - 2u_e v_e \phi - u_e^2\psi + \lambda\phi = 0, & \text{(3.1a)} \\ D(-\Delta)^{s_2}\psi + \dfrac{2}{\varepsilon}Au_e v_e\phi + \dfrac{1}{\varepsilon}Au_e^2\psi + \varepsilon\lambda\psi = 0. & \text{(3.1b)} \end{cases}$$

Let $\phi(x_i + \varepsilon y) \sim \Phi_i(y)$ and $\psi(x_i + \varepsilon y) \sim \Psi_i(y)$ to deduce the inner problem

$$\begin{cases} (-\Delta)^{s_1}\Phi_i + \Phi_i - 2w\Phi_i - \xi_i^2 w^2 \Psi_i + \lambda\Phi_i = 0, & -\frac{1+x_i}{\varepsilon} < y < \frac{1-x_i}{\varepsilon}, \quad \text{(3.2a)} \\ D(-\Delta)^{s_2}\Psi_i + 2\varepsilon^{2s_2-1}Aw\Phi_i + \varepsilon^{2s_2-1}A\xi_i^2 w^2\Psi_i + \varepsilon^{2s_2+1}\lambda\Psi_i = 0, & -\frac{1+x_i}{\varepsilon} < y < \frac{1-x_i}{\varepsilon}. \quad \text{(3.2b)} \end{cases}$$

We deduce that Ψ_i is constant to leading order. Moreover, the distributional limits (2.5) and

$$\frac{1}{\varepsilon}u_e v_e \phi \longrightarrow \sum_{j=1}^{N}\int_{-\infty}^{\infty} w\Phi_j dy \delta(x - x_j),$$

yield the leading order outer problem

$$D(-\Delta)^{s_2}\psi + A\sum_{j=1}^{N}\left(2\int_{-\infty}^{\infty} w(y)\Phi_i(y)dy + \omega\xi_j^2\Psi_j\right)\delta(x - x_j) = 0.$$

Provided the solvability condition

$$2\sum_{j=1}^{N}\int_{-\infty}^{\infty} w(y)\Phi_i(y)dy + \omega\sum_{j=1}^{N}\xi_j^2\Psi_j = 0, \tag{3.3}$$

is satisfied, we thus deduce that

$$\psi(x) \sim \frac{A}{D}\sum_{j=1}^{N}\left(2\int_{-\infty}^{\infty} w(y)\Phi_i(y)dy + \omega\xi_j^2\Psi_j\right)G(x - x_j) + \gamma,$$

where γ is an undetermined constant. The resulting matching condition is then

$$\Psi_i = \frac{A}{D}\sum_{j=1}^{N}\left(2\int_{-\infty}^{\infty} w(y)\Phi_i(y)dy + \omega\xi_j^2\Psi_j\right)G(x_i - x_j) + \gamma. \tag{3.4}$$

Together with the solvability condition (3.3) this can be solved for the unknowns $\Psi_1, ..., \Psi_N$ and γ.

For the purposes of this paper it will suffice to consider the resulting expression only in the case of symmetric N spike solutions. In such a case we can rewrite (3.3) and (3.4) as

$$\begin{cases} 2\boldsymbol{e}_N^T\displaystyle\int_{-\infty}^{\infty} w(y)\boldsymbol{\Phi}(y)dy + \omega\xi_c^2\boldsymbol{e}_N^T\boldsymbol{\Psi} = 0, & \text{(3.5a)} \\ \left(\mathcal{I}_N - \dfrac{A\omega\xi_c^2}{D}\mathcal{G}\right)\boldsymbol{\Psi} = \dfrac{2A}{D}\mathcal{G}\displaystyle\int_{-\infty}^{\infty} w(y)\boldsymbol{\Phi}(y)dy + \gamma\boldsymbol{e}_N, & \text{(3.5b)} \end{cases}$$

where $\mathcal{I}_N$ is the $N \times N$ identity matrix and $\boldsymbol{\Phi} = (\Phi_1, ..., \Phi_N)^T$. Left multiplying the second equation by $\boldsymbol{e}_N^T$ and using the first equation together with (2.17b) we deduce

$$\gamma = -\frac{2}{N\omega\xi_c^2}\boldsymbol{e}_N^T\int_{-\infty}^{\infty} w(y)\boldsymbol{\Phi}(y)dy.$$

We thus obtain

$$\boldsymbol{\Psi} = 2\left(\mathcal{I}_N - \frac{A\omega\xi_c^2}{D}\mathcal{G}\right)^{-1}\left(\frac{A}{D}\mathcal{G} - \frac{1}{\omega\xi_c^2}\mathcal{E}_N\right)\int_{-\infty}^{\infty} w(y)\boldsymbol{\Phi}(y)dy, \tag{3.6}$$

where we define the rank one matrix

$$\mathcal{E}_N := \frac{1}{N}\boldsymbol{e}\boldsymbol{e}_N^T. \tag{3.7}$$

Substituting this into (3.2a) we obtain the nonlocal eigenvalue problem (NLEP)

$$(-\Delta)^{s_1}\boldsymbol{\Phi} + \boldsymbol{\Phi} - 2w\boldsymbol{\Phi} - 2\mathcal{B}\frac{\int_{-\infty}^{\infty} w(y)\boldsymbol{\Phi}(y)dy}{\int_{-\infty}^{\infty} w(y)^2 dy}w^2 + \lambda\boldsymbol{\Phi} = 0, \tag{3.8a}$$

where

$$\mathcal{B} = \left(\mathcal{I}_N - \frac{A\omega\xi_c^2}{D}\mathcal{G}\right)^{-1}\left(\frac{A\omega\xi_c^2}{D}\mathcal{G} - \mathcal{E}_N\right). \tag{3.8b}$$

The matrices $\mathcal{G}$ and $\mathcal{E}_N$ appearing in (3.8b) are both circulant so they share the same eigenvectors and their eigenvalues can be computed explicitly as in Appendix B. Specifically, since $\mathcal{G}$ is symmetric its eigenvalues are real and given by

$$\sigma_k(\mathcal{G}) = G(0) + \sum_{j=1}^{N-1} G(2j/N)\cos(2\pi jk/N), \qquad k = 0, ..., N-1. \tag{3.9}$$

On the other hand, it is straightforward to check that $\sigma_k(\mathcal{E}_N) = \delta_{k0}$ for $k = 0, ..., N-1$. The eigenvalues of $\mathcal{B}$ can thus be readily computed and are explicitly given by

$$\sigma_k(\mathcal{B}) = -\frac{\delta_{k0} - A\omega\xi_c^2 D^{-1}\sigma_k(\mathcal{G})}{1 - A\omega\xi_c^2 D^{-1}\sigma_k(\mathcal{G})}, \qquad k = 0, ..., N-1. \tag{3.10}$$

We can thus diagonalize the NLEP system (3.8a) to obtain the scalar NLEPs

$$(-\Delta)^{s_1}\Phi_k + \Phi_k - 2w\Phi_k - 2\sigma_k(\mathcal{B})\frac{\int_{-\infty}^{\infty} w(y)\Phi_k(y)dy}{\int_{-\infty}^{\infty} w(y)^2 dy}w^2 + \lambda\Phi_k = 0, \qquad k = 0, ..., N-1, \tag{3.11}$$

which determine the linear stability with respect to k^{th}-mode perturbations of the form $\boldsymbol{\Phi}_k = \phi(y)\boldsymbol{v}_k$ where $\boldsymbol{v}_k$ is the eigenvector corresponding to $\sigma_k(\mathcal{B})$ (see Appendix B). By Theorem 3.2 in [8] we deduce that the scalar NLEP (3.11) is unstable (i.e. $\text{Re}\lambda > 0$) if $\sigma_k(\mathcal{B}) > -1/2$ and is stable when $\sigma_k(\mathcal{B}) < -1/2$. In particular, we deduce that the symmetric N-spike solution is stable with respect to k^{th}-mode perturbations provided that

$$\max_{k=1,...,N-1}\sigma_k(\mathcal{B}) < -\frac{1}{2}, \tag{3.12}$$

where we have used $\sigma_0(\mathcal{B}) = -1$ to restrict the maximization to $k = 1, ..., N-1$. We numerically find that $\sigma_k(\mathcal{G}) < 0$ for all $k = 1, ..., N-1$ so that

$$\max_{k=1,...,N-1}\sigma_k(\mathcal{B}) = \max_{k=1,...,N-1} -\frac{A\omega\xi_c^2 D^{-1}|\sigma_k(\mathcal{G})|}{1 + A\omega\xi_c^2 D^{-1}|\sigma_k(\mathcal{G})|}.$$

Taking $D \to \infty$ we determine that the symmetric N-spike solution is always linearly unstable, whereas it is linearly stable provided $D > 0$ is sufficiently small. In particular, we deduce that the unique stability threshold $D = D_N^{\text{large}}$ is given by

$$D_N^{\text{large}} = \min_{k=1,...,N-1} D_{N,k}^{\text{large}}, \qquad D_{N,k}^{\text{large}} := \frac{1}{N^2 A\omega}|\sigma_k(\mathcal{G})|, \tag{3.13}$$

in terms of which the symmetric N-spike solution is linearly stable with respect to the large eigenvalues provided that $D < D_N^{\text{large}}$. In Figure 1 we plot the large eigenvalue thresholds $D_{N,k}^{\text{large}}$ for

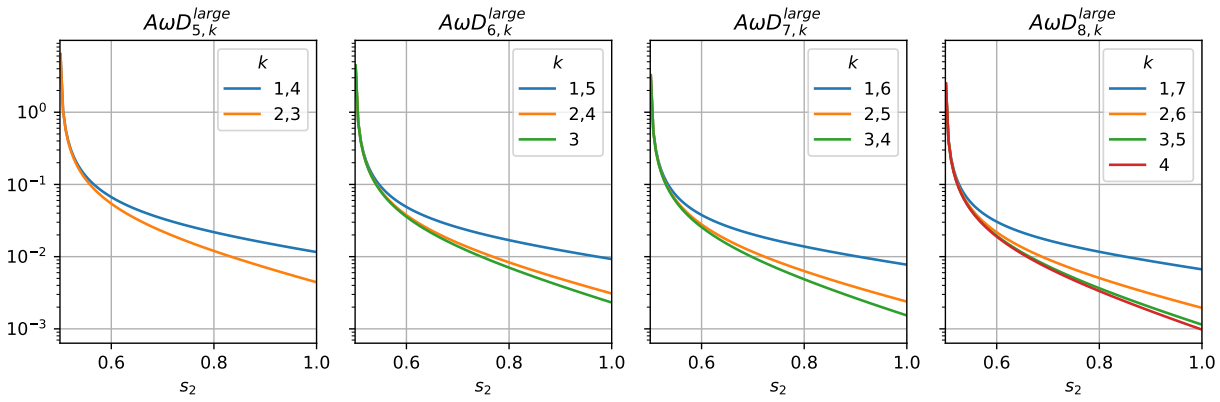

FIGURE 1. Large eigenvalue stability thresholds $D^{\text{large}}_{N,k}$. Note that all plots share a common y-axis indicated by the left-most figure.

$N = 5, 6, 7, 8$ versus s_2. Note that the rescaled thresholds plotted in this figure are independent of A and s_1 since the s_1 dependence arises only through the factor ω. Note that, in contrast to the $s_2 = 1$ case, the large eigenvalue thresholds for distinct modes appear to merge as $s_2 \to 0.5^+$. Finally, in Figure 3a we plot the large eigenvalue thresholds D^{large}_N together with small eigenvalue thresholds to be further discussed in the next section.

4. Slow Dynamics and the Small Eigenvalues

Spike solutions of a variety of classical singularly perturbed reaction-diffusion systems are known to exhibit slow dynamics over a long time scale. The same phenomenon likewise holds for the one-dimensional fractional Gierer-Meinhardt system as described in [8]. In this section we determine the slow dynamics of spike solutions to (1.1) and by then studying the linear stability of the resulting ODE system we will determine the eigenvalue problem satisfied by the small eigenvalues. Throughout this section we assume that the quasi-equilibrium solution is linearly stable with respect to the large eigenvalues.

We begin by first refining the limiting behaviour of the outer solution (2.15a) as $x \to x_i$. Specifically, using (2.11) we find that

$$v_e(x_i + \varepsilon y) \sim \frac{A\omega}{D}\sum_{j=1}^{N}\xi_j G(x_i - x_j) + \chi - \frac{A\omega\xi_i}{D}\mathfrak{a}_{s_2}|y|^{2s_2-1}\varepsilon^{2s_2-1} + \frac{\varepsilon A}{D}\omega\beta_i y, \tag{4.1}$$

where $\beta_i = \sum_{j\neq i}\xi_j G'(x_i - x_j)$. Now we suppose that $x_i = x_i(t)$ and consider the higher order inner expansions $u(x_i + \varepsilon y) \sim \xi_i + U_{i1}$ and $v(x_i + \varepsilon y) \sim \xi_i^{-1} + V_{i1}$ where $U_{i1} \ll 1$ and $V_{i1} \ll 1$ satisfy

$$\begin{cases} -\varepsilon^{-1}\xi_i\dfrac{dx_i}{dt}w' + (-\Delta)^{s_1}U_i + U_i - 2wU_{i1} - \xi_i^2 w^2 V_{i1} + \text{h.o.t} = 0, & \text{(4.2a)} \\ D(-\Delta)^{s_2}V_{i1} + \varepsilon^{2s_2-1}A\xi_i w^2 + \text{h.o.t} = 0. & \text{(4.2b)} \end{cases}$$

Matching the far-field behaviour of V_{i1} with (4.1) we find that V_{i1} must satisfy

$$V_{i1} \sim -\frac{A\omega\xi_i}{D}\mathfrak{a}_{s_2}|y|^{2s_2-1}\varepsilon^{2s_2-1} + \frac{\varepsilon A\omega}{D}\beta_i y, \qquad |y| \to \infty.$$

We write $V_{i1}(y) = \varepsilon A\omega D^{-1}\beta_i y + \varepsilon^{2s_2-1}\tilde{V}_{i1} + o(\varepsilon)$, where $\tilde{V}_{i1}$ is an even function in y and to leading order is given by

$$\tilde{V}_{i1} = -A\xi_i D^{-1}(-\Delta)^{-s_2}w + o(1). \tag{4.3}$$

Since $(-\Delta)^{s_2} y = 0$ we deduce that such a V_{i1} does indeed satisfy (4.2b). Moreover by taking Fourier transforms we find that

$$(-\Delta)^{-s_2} w = C + \mathfrak{a}_{s_2} \int_{-\infty}^{\infty} |y-z|^{2s_2-1} w(y)^2 dy \longrightarrow C + \mathfrak{a}_{s_2} |y|^{2s_2-1} \omega, \quad |y| \to \infty,$$

so that V_{i1} also has the desired far-field behaviour. Substituting V_{i1} into (4.2a) then gives

$$-\varepsilon^{-1} \xi_i \frac{dx_i}{dt} w' + \mathscr{L} U_{i1} - \varepsilon \xi_i^2 A \omega D^{-1} \beta_i y w^2 - \varepsilon^{2s_2-1} \xi_i^2 w^2 \tilde{V}_{i1} + \text{h.o.t} = 0, \tag{4.4}$$

where the linear operator $\mathscr{L}$ is defined by

$$\mathscr{L}\phi := (-\Delta)^{s_1} \phi + \phi - 2w\phi. \tag{4.5}$$

Multiplying (4.4) by w' and integrating then gives

$$-\frac{\xi_i}{\varepsilon} \frac{dx_i}{dt} \int_{-\infty}^{\infty} |w'|^2 dy - \frac{\varepsilon \xi_i^2 A\omega}{D} \beta_i \int_{-\infty}^{\infty} y w' w^2 dy + \text{h.o.t} = 0,$$

where we have used the fact that w' is odd and satisfies $\mathscr{L} w' = 0$ to deduce $\int_{-\infty}^{\infty} w' \mathscr{L} U_{i1} dy = \int_{-\infty}^{\infty} U_{i1} \mathscr{L} w' dy = 0$ and $\int_{-\infty}^{\infty} w' \tilde{V}_{i1} dy = 0$.

The leading order slow dynamics of the N spike quasi-equilibrium solution (2.15a) are thus determined by the ODE system

$$\frac{d\boldsymbol{x}}{dt} = \varepsilon^2 \frac{A\omega \int_{-\infty}^{\infty} w^3 dy}{3D \int_{-\infty}^{\infty} |w'|^2 dy} \begin{pmatrix} \xi_1 & & 0 \\ & \ddots & \\ 0 & & \xi_N \end{pmatrix} \boldsymbol{\beta}, \tag{4.6}$$

where

$$\boldsymbol{x} = (x_1, ..., x_N)^T, \qquad \boldsymbol{\beta} = \nabla_{\boldsymbol{x}} \mathcal{G} \boldsymbol{\xi}, \tag{4.7}$$

and $\nabla_{\boldsymbol{x}} \mathcal{G}$ is the $N \times N$ matrix with entries

$$(\nabla_{\boldsymbol{x}} \mathcal{G})_{ij} = \begin{cases} 0, & i = j, \\ G'(x_i - x_j), & \text{otherwise.} \end{cases} \tag{4.8}$$

This system of ODEs (4.6) is to be solved together with the NAS (2.15b) and therefore constitutes a differential algebraic system (DAE). We remark that since $G'(z) \gtrless 0$ for $z \gtrless 0$ the spikes are mutually repelling. Moreover, an N-spike solution is in equilibrium provided that $\beta_i = 0$ for all $i = 1, ..., N$. From symmetry considerations it is straightforward to see that the symmetric N-spike solution of §2.1 with (2.17) satisfies these conditions and is therefore in equilibrium.

4.1. **Small Eigenvalues for Symmetric N-Spike Solutions.** We now consider the linear stability of the symmetric N-spike solution from §2.1 with respect to the *small* eigenvalues. We remind the reader that by a symmetric solution we mean one for which $\boldsymbol{\xi} = \xi_c \boldsymbol{e}_N^T$ where ξ_c is given by (2.16) and where the spike locations are given by (2.17a). The small eigenvalues are determined by studying the linear stability of the N-spike solution over an $O(\varepsilon^{-2})$ timescale. Specifically, we seek eigenvalues of the linearization of the slow dynamics (4.6). Since $\boldsymbol{\beta} = 0$ for an equilibrium solution, it suffices to calculate the eigenvalues of the $N \times N$ matrix

$$\mathcal{H} := \nabla_{\boldsymbol{x}} (\nabla_{\boldsymbol{x}} \mathcal{G} \boldsymbol{\xi}) = (\nabla_{\boldsymbol{x}} \mathcal{G})(\nabla_{\boldsymbol{x}} \boldsymbol{\xi}) + \xi_c \mathcal{Q},$$

where $\nabla_{\boldsymbol{x}} \mathcal{G}$ is given by (4.8) while $\nabla_{\boldsymbol{x}} \boldsymbol{\xi}$ and $\mathcal{Q}$ are the $N \times N$ matrices with entries

$$(\nabla_{\boldsymbol{x}} \boldsymbol{\xi})_{ij} = \frac{\partial \xi_i}{\partial x_j}, \qquad \mathcal{Q}_{ij} = \begin{cases} \sum_{l \neq i} G''(x_i - x_l), & i = j, \\ -G''(x_i - x_j), & \text{otherwise.} \end{cases} \tag{4.9}$$

It thus remains to find $\nabla_{\boldsymbol{x}}\boldsymbol{\xi}$ for which we turn our attention to the NAS (2.15b). First, by differentiating the solvability condition (2.7) with respect to the spike locations we deduce that $\boldsymbol{e}^T\nabla_{\boldsymbol{x}}\boldsymbol{\xi} = 0$ and hence

$$\nabla_{\boldsymbol{x}}\chi\boldsymbol{e}_N = -2ND^{-1}\mu_N\xi_c(A\omega)^2\mathcal{E}_N\nabla_{\boldsymbol{x}}\boldsymbol{\xi} = 0,$$

where we have also used the fact that $\sum_{j\neq i}G'(x_i - x_j) = 0$ for all $i = 1, ..., N$. It is then straightforward to differentiate the NAS (2.15b) to deduce that

$$\nabla_{\boldsymbol{x}}\boldsymbol{\xi} = \frac{\xi_c^2}{DN}\left(\mathcal{I}_N + \frac{\xi_c}{DN}\mathcal{G}\right)^{-1}\nabla_{\boldsymbol{x}}\mathcal{G}.$$

With the above equations we finally conclude that

$$\mathcal{H} = \frac{\xi_c^2}{DN}\nabla_{\boldsymbol{x}}\mathcal{G}\left(\mathcal{I}_N + \frac{\xi_c}{DN}\mathcal{G}\right)^{-1}\nabla_{\boldsymbol{x}}\mathcal{G} + \xi_c\mathcal{Q}. \tag{4.10}$$

Note that the matrices $\mathcal{G}$, $\nabla_{\boldsymbol{x}}\mathcal{G}$, and $\mathcal{Q}$ are each circulant so they share the same eigenvectors and their eigenvalues can be computed explicitly as in Appendix B. Specifically, the eigenvalues of $\mathcal{G}$ are explicitly given by (3.9) whereas those of $\nabla_{\boldsymbol{x}}\mathcal{G}$ and $\mathcal{Q}$ are respectively given by

$$\sigma_k(\nabla_{\boldsymbol{x}}\mathcal{G}) = i\sum_{j=1}^{N-1}G'(2j/N)\sin(2\pi jk/N), \qquad k = 0, ..., N-1, \tag{4.11}$$

$$\sigma_k(\mathcal{Q}) = \sum_{j=1}^{N-1}G''(2j/N)\left(1 - \cos(2\pi jk/N)\right), \qquad k = 0, ..., N-1. \tag{4.12}$$

The eigenvalues of $\mathcal{H}$ are therefore given by

$$\sigma_k(\mathcal{H}) = \xi_c^2\frac{\sigma_k(\nabla_{\boldsymbol{x}}\mathcal{G})^2}{DN + \xi_c\sigma_k(\mathcal{G})} + \xi_c\sigma_k(\mathcal{Q}), \qquad k = 0, ..., N-1.$$

Observe that $\sigma_0(\nabla_{\boldsymbol{x}}\mathcal{G}) = \sigma_0(\mathcal{Q}) = 0$ so that $\sigma_0(\mathcal{H}) = 0$. This neutrally stable $k = 0$ mode is a consequence of the translational invariance of the system (1.1). Recalling our definition of the large eigenvalue stability thresholds $D_{N,k}^{\text{large}}$ from (3.13) we rewrite the expression for $\sigma_k(\mathcal{H})$ as

$$\sigma_k(\mathcal{H}) = \frac{1}{N^3A^2\omega^2}\frac{\sigma_k(\nabla_{\boldsymbol{x}}\mathcal{G})^2}{D - D_{N,k}^{\text{large}}} + \frac{1}{NA\omega}\sigma_k(\mathcal{Q}), \qquad k = 1, ..., N-1,$$

in which stability with respect to the large eigenvalues implies that $D < D_{N,k}^{\text{large}}$ for all $k = 1, ..., N-1$. Note that by the symmetry properties of the matrices involved in the above definition we have $\sigma_k(\mathcal{H}) = \sigma_{N-k}(\mathcal{H})$ so that we need only consider the values $k = 1, ..., \lfloor N/2\rfloor$ where $\lfloor z\rfloor$ denotes the largest integer $\leq z$.

We make the following observation regarding the small eigenvalue thresholds. First, since $\nabla_{\boldsymbol{x}}\mathcal{G}$ is skew-symmetric we deduce from (B.5) that $\sigma_k(\nabla_{\boldsymbol{x}}\mathcal{G}) = 0$ when N is even and $k = N/2$. Otherwise, we numerically find that $\sigma_k(\nabla_{\boldsymbol{x}}\mathcal{G})^2 < 0$. On the other hand, numerical calculations indicate that $\sigma_k(\mathcal{Q}) < 0$ for all $k = 1, ..., N-1$ for any $N \geq 2$. Thus, if N is even then the $k = N/2$ small eigenvalue is always linearly stable. In particular we deduce that for $N = 2$ we have $\sigma_0(\mathcal{H}) = 0$ and $\sigma_1(\mathcal{H}) < 0$ so that $N = 2$-spike solutions are linearly stable with respect to the small eigenvalues and their overall linear stability is therefore dictated solely by the large eigenvalues.

Turning our attention next to $N \geq 3$ we deduce that the N-spike solution is linearly stable with respect to the k^{th} small eigenvalue provided that $D < D_{N,k}^{\text{small}}$ where

$$D_{N,k}^{\text{small}} := D_{N,k}^{\text{large}} - \frac{1}{N^2A\omega}\frac{\sigma_k(\nabla_{\boldsymbol{x}}\mathcal{G})^2}{\sigma_k(\mathcal{Q})} \leq D_{N,k}^{\text{large}}. \tag{4.13}$$

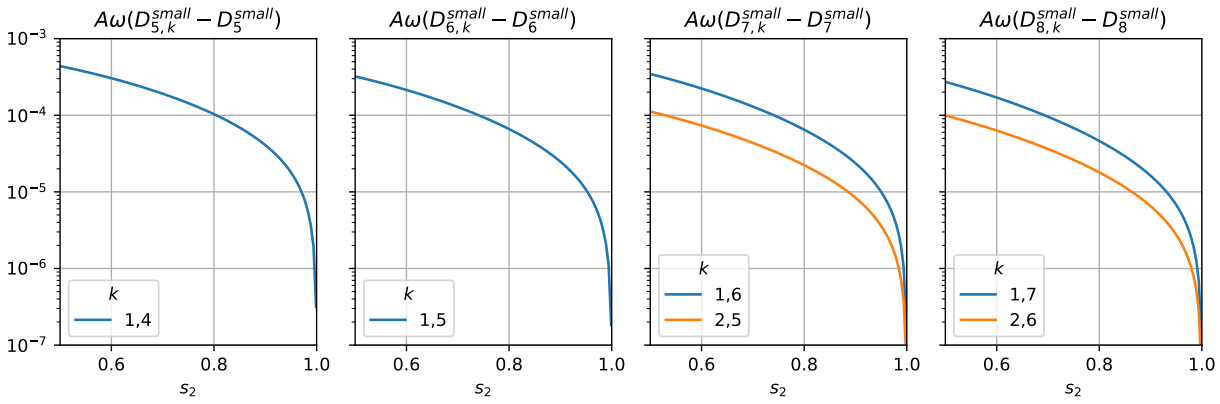

FIGURE 2. Small eigenvalue stability thresholds $D^{\text{small}}_{N,k}$. Note that all plots share a common y-axis indicated by the left-most figure.

Note that this equation no longer holds if N is even and $k = N/2$. Stability with respect to the small eigenvalues is determined by the minimum of $D^{\text{small}}_{N,k}$ over all $k = 1, ..., \lfloor N/2 \rfloor$ if N is odd and $k = 1, ..., N/2 - 1$ if N is even. In fact, numerical calculations indicate that these minima are attained at $k = \lfloor N/2 \rfloor$ for odd N and $k = N/2 - 1$ for even N. Letting

$$D^{\text{small}}_N = \begin{cases} D^{\text{small}}_{N,\lfloor N/2 \rfloor}, & N \text{ odd}, \\ D^{\text{small}}_{N,N/2-1}, & N \text{ even}, \end{cases} \tag{4.14}$$

then we immediately deduce that if N is odd then $D^{\text{small}}_N < D^{\text{large}}_N$. On the other hand, numerical calculations indicate that if N is even then $D^{\text{large}}_N < D^{\text{small}}_N$ (see Figures 3c and 3b). We therefore deduce that whereas it is the small eigenvalues that dictate the linear stability of N-spike solutions when N is odd, it is instead the large eigenvalues that dictate the linear stability when N is even. Note that for even N the inequality $D^{\text{small}}_{N,k} < D^{\text{large}}_{N,k}$ still holds for all $k = 1, ..., N/2 - 1$, but in this case all these small eigenvalue thresholds exceed $D^{\text{large}}_{N,N/2}$. We remark that in the case $s_2 = 1$ we find that if N is even then $D^{\text{small}}_N = D^{\text{large}}_N$, i.e. the small- and large-eigenvalue thresholds coincide. However, this equality is broken if periodic boundary conditions are replaced with Neumann boundary conditions in which case the small eigenvalues always dictate the linear stability [27]. Indeed, apart from periodic boundary conditions, the slow dynamics and linear stability are known to be affected by interactions with the boundary [27, 11].

We summarize the results from the previous two sections in the following proposition.

Proposition 4.1. *Suppose that $\varepsilon \ll 1$ and let u_e and v_e be the symmetric N-spike solution in Proposition 2.1 with spike locations $x_1, ..., x_N$ given by (2.17a) and a common spike height $\xi_c = (NA\omega)^{-1}$. Then u_e and v_e are equilibrium solutions of (1.1) and they are linearly stable with respect to both the large and small eigenvalues if and only if*

$$D < \begin{cases} D^{large}_N = \frac{1}{N^2 A\omega} |\sigma_{N/2}(\mathcal{G})|, & \text{if } N \text{ is even}, \\ D^{small}_N = \frac{1}{N^2 A\omega} \left(|\sigma_{(N-1)/2}(\mathcal{G})| - \frac{\sigma_{(N-1)/2}(\nabla_{\boldsymbol{x}} \mathcal{G})^2}{\sigma_{(N-1)/2}(\mathcal{Q})} \right), & \text{if } N \text{ is odd}. \end{cases} \tag{4.15}$$

In Figure 2 we plot the difference $A\omega(D^{\text{small}}_{N,k} - D^{\text{small}}_N)$ for $N = 5, 6, 7, 8$. Note that the small eigenvalue thresholds differ for different modes for $s_2 < 1$. This is in stark contrast to the classical $s_2 = 1$ case. Some of the consequences of this behaviour on the existence of asymmetric solutions are numerically investigated in §5 below. In §6 we observe a similar behaviour for the small eigenvalues

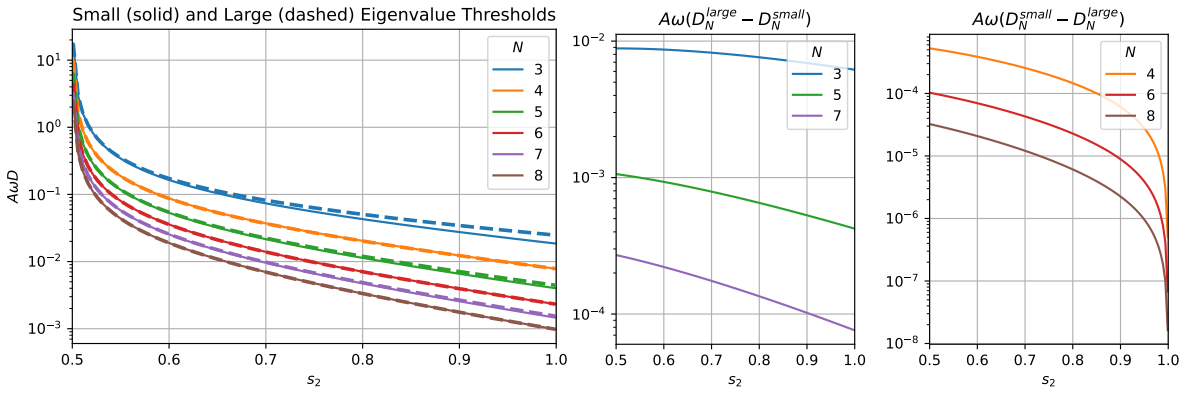

(A) (B) (C)

FIGURE 3. (A) Small and large eigenvalue stability thresholds D_N^{small} and D_N^{large} versus s_2. (B) Difference between the large and small eigenvalue thresholds for odd N, and (C) difference between the small and large eigenvalue thresholds for even N.

of the fractional Gierer-Meinhardt system. This behaviour appears to be unique to fractional reaction-diffusion systems though the reasons for this peculiar behaviour are not presently well understood. We conclude this section by plotting in Figure 3a both the small and large eigenvalue thresholds versus s_2 for $N = 5, 6, 7, 8$. As expected we see that for even values of N the small eigenvalue threshold (just barely) exceeds the large eigenvalue threshold whereas for odd values of N the opposite is (more pronouncedly) the case.

5. Asymmetric Solutions and the Small Eigenvalues

Classical singularly perturbed reaction diffusion systems like the Schnakenberg and Gierer-Meinhardt systems are known to exhibit not only symmetric N-spike solutions, but also asymmetric N-spike solutions [26, 27]. Although the stability of such asymmetric solutions often requires the numerical computation of eigenvalues of certain matrices, their construction is remarkably tractable. Specifically, a complete characterization of asymmetric N-spike solutions can be achieved by using a *gluing method* in which solutions to the same problem in a domain of variable length are *glued* together [26, 27]. However, this method relies crucially on the local nature of the classical Laplacian and is therefore not applicable in the fractional Laplacian case.

Although we can't analytically construct asymmetric solutions to the fractional system (1.1) with the gluing method discussed above, we can obtain such asymmetric solutions using a numerical continuation starting from the symmetric N-spike solutions considered in §2.1, and the small-eigenvalue thresholds $D_{N,k}^{\text{small}}$. Indeed, each of the small eigenvalue thresholds $D_{N,k}^{\text{small}}$ correspond to bifurcation points from the symmetric N-spike solution to the $2N$-dimensional nonlinear system consisting of the NAS (2.15b) and equilibrium system for the DAE (4.6), i.e.

$$\boldsymbol{\xi}^{-1} - \frac{A\omega}{D}\mathcal{G}\boldsymbol{\xi} + \chi \boldsymbol{e}_N = 0, \qquad \nabla_{\boldsymbol{x}}\mathcal{G}\boldsymbol{\xi} = 0. \tag{5.1}$$

Using the numerical continuation sub-package `PyCont` of `PyDSTool` [2] we numerically calculate bifurcation diagrams for the system (5.1) when $A = 1$, $s_1 = 0.5$ and $s_2 = 0.7, s_2 = 0.9$. The resulting bifurcation diagrams are shown in Figures 4a and 5a for $s_2 = 0.7$ and $s_2 = 0.9$ respectively. In these diagrams we plot $\|\boldsymbol{\xi}\|_2^2 := \sum_{i=1}^N \xi_i^2$ versus D for $N = 2, 3, 4, 5$-spike solutions. The solid (resp. dotted) horizontal lines indicate symmetric N-spike solutions that are stable (resp. unstable) with

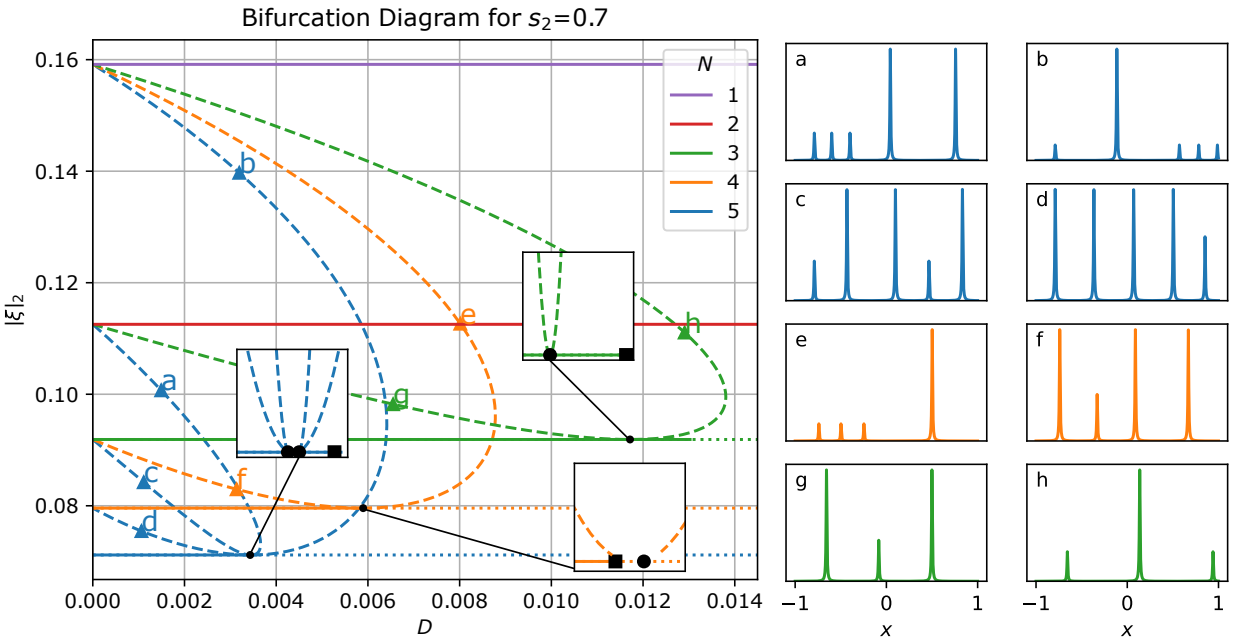

FIGURE 4. (A) Bifurcation diagram for $s_2 = 0.7$ plotting $\|\boldsymbol{\xi}\|_2$ versus D. The colours indicate the number of spikes in each solution as per the legend. Solid (resp. dotted) horizontal lines indicate symmetric N spike solutions that are stable (resp. unstable) with respect to the $O(1)$ eigenvalues. Dashed lines indicate asymmetric N-spike solutions whose linear stability is undetermined. The insets provide a close up of the points where asymmetric solutions bifurcate from the symmetric ones. (B) Plots of the asymptotically calculated equilibrium solution $u_e(x)$ for sample asymmetric N-spike solutions at the labelled ▲ points in (A).

respect to the $O(1)$ eigenvalues. The large eigenvalue threshold for the $N = 2$ curve appears at a larger value of D and is not here shown. The dashed curves branching out of the symmetric solution branches correspond to asymmetric solutions. The insets in both of these figures show a close up of the regions where asymmetric branches bifurcate from the symmetric ones. In these insets the circles and square respectively indicate the small and large eigenvalue thresholds. Additionally, in Figures 4b and 5b we plot the asymptotically calculated equilibrium solution $u_e(x)$ when $\varepsilon = 0.005$ at the corresponding triangle markers on bifurcation diagram.

We draw particular attention to the insets at the $N = 5$ bifurcation points for which we see that there are two distinct points from which asymmetric solutions bifurcate, with this difference being more pronounced in the $s_2 = 0.7$ case in Figure 4a as opposed to the $s_2 = 0.9$ case in Figure 5a. In addition, from the insets around the $N = 4$ bifurcation point we see that the large eigenvalue threshold is to the left of the small eigenvalue threshold in contrast to the (odd) values of $N = 3$ and $N = 5$. Finally, we remark that numerical simulations of the full system (1.1) (not shown) starting from the asymmetric N-spike solutions suggest that these solutions are linearly unstable. This is inline with the theoretical predictions obtained in [27] for the classical two-dimensional Schnakenberg system in which it was shown that asymmetric solutions always have an unstable small, $O(\varepsilon^2)$ eigenvalue. We leave a systematic study of the linear stability of asymmetric solutions to (1.1) for future work.

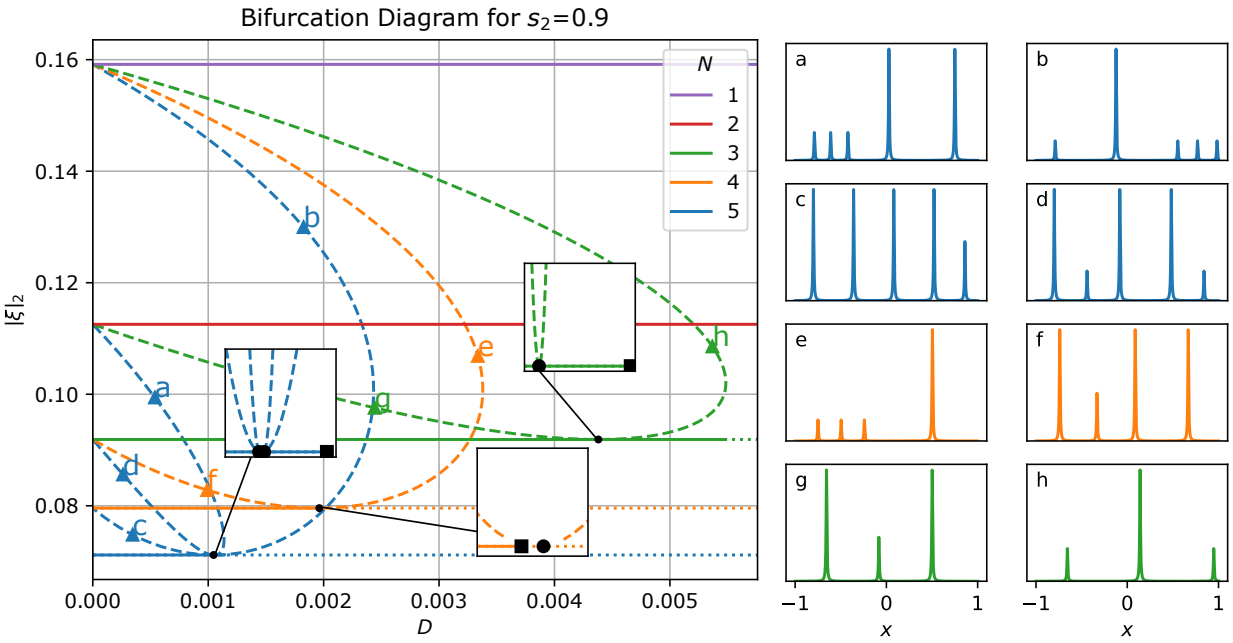

FIGURE 5. (A) Bifurcation diagram for $s_2 = 0.9$, and (B) accompanying sample asymmetric solutions. See Figure 4 for further details.

6. Small Eigenvalues for the Fractional Gierer-Meinhardt System

Proceeding as for the Schnakenberg system above, we here briefly consider the linear stability of multi-spike solutions to the fractional Gierer-Meinhardt system

$$\begin{cases} u_t + \varepsilon^{2s_1}(-\Delta)^{s_1}u + u - u^2v^{-1} = 0 & -1 < x < 1, \qquad (6.1a) \\ \tau v_t + D(-\Delta)^{s_2}v + v - u^2 = 0, & -1 < x < 1, \qquad (6.1b) \\ u(x+2) = u(x), \qquad v(x+2) = v(x), & x \in \mathbb{R}, \qquad (6.1c) \end{cases}$$

where we assume $1/4 < s_1 < 1$ and $1/2 < s_2 < 1$. The existence and linear stability of two-spike solutions, both symmetric and asymmetric, was previously considered in [8]. Here we summarize the results of the asymptotic analysis that characterizes the equilibrium solutions and their linear stability. Specifically, following the method of matched asymptotic expansions we find that equilibrium solutions take the form

$$u_e(x) \sim \varepsilon^{-1}\sum_{j=1}^{N}\xi_j w\left(\frac{x-x_j}{\varepsilon}\right), \qquad v_e(x) \sim \varepsilon^{-1}\omega\sum_{j=1}^{N}\xi_j^2 G_D(x-_j),$$

where $w(y)$ is the fractional-homoclinic satisfying (2.4), $\omega = \int_{-\infty}^{\infty} w(y)^2 dy$, and $G_D(x)$ is the fractional 2-periodic Green's function satisfying

$$D(-\Delta)^{s_2}G_D(x) + G_D(x) = \delta(x), \quad -1 < x < 1; \qquad G_D(x) = G_D(x+2), \quad x \in \mathbb{R}.$$

A rapidly converging series expansion of this Green's function can be found in Appendix C of [8]. The values $\boldsymbol{\xi} = (\xi_1, ..., \xi_N)^T$ are determined by the matching conditions which take the form

$$\boldsymbol{\xi} - \omega\mathcal{G}_D\boldsymbol{\xi}^2 = 0, \qquad (6.2)$$

where $\mathcal{G}_D$ is the $N \times N$ matrix with entries $(\mathcal{G}_D)_{ij} = G_D(x_i - x_j)$.

The equilibrium positions are determined by the slow dynamics ODE which takes the form

$$\frac{d\boldsymbol{x}}{dt} = -\varepsilon^2 \frac{\int_{-\infty}^{\infty} w^2 dy \int_{-\infty}^{\infty} w^3 dy}{3\int_{-\infty}^{\infty} |dw/dy|^2 dy} \begin{pmatrix} \xi_1^{-1} & & 0 \\ & \ddots & \\ 0 & & \xi_N^{-1} \end{pmatrix} \nabla_{\boldsymbol{x}} \mathcal{G}_D \boldsymbol{\xi}^2.$$

where $\boldsymbol{x} = (x_1, ..., x_N)^T$ and $\nabla_{\boldsymbol{x}} \mathcal{G}_D$ is the $N \times N$ matrix with entries

$$(\nabla_{\boldsymbol{x}} \mathcal{G}_D)_{ij} = \begin{cases} 0, & i = j, \\ G_D'(x_i - x_j), & \text{otherwise.} \end{cases}$$

As for the Schnakenberg system above, we can construct symmetric N-spike solutions by assuming $x_1, ..., x_N$ are distributed according to (2.17a). With this choice of spike locations the matrix $\mathcal{G}_D$ is again circulant and we can read off its eigenvalues $\sigma_0(\mathcal{G}_D), ..., \sigma_{N-1}(\mathcal{G}_D)$ as in Appendix B. Substituting $\boldsymbol{\xi} = \xi_c \boldsymbol{e}$ into (6.2) then gives the common spike height $\xi_c = (\omega \sigma_0(\mathcal{G}_D))^{-1}$.

The linear stability of a symmetric N-spike pattern (with $\tau = 0$ to avoid Hopf bifurcations) with respect to the large eigenvalues is determined by the NLEPs

$$(-\Delta)^{s_1} \Phi_k + \Phi_k + 2\frac{\sigma_k(\mathcal{G}_D)}{\sigma_0(\mathcal{G}_D)} \frac{\int_{-\infty}^{\infty} w(y)\Phi_k(y) dy}{\int_{-\infty}^{\infty} w(y)^2 dy} + \lambda \Phi_k = 0,$$

for $k = 0, ..., N-1$. By Theorem 3.2 of [8] the eigenvalue in the k^{th} NLEP above will be stable if and only if

$$2\sigma_k(\mathcal{G}_D) > \sigma_0(\mathcal{G}_D).$$

Thus for $k = 0$ the NLEP is always linearly stable and we can otherwise determine the large eigenvalue thresholds $D_{k,N}^{\text{large}}$ by solving $2\sigma_k(\mathcal{G}_D) - \sigma_0(\mathcal{G}_D) = 0$. In particular the symmetric N-spike solution is linearly stable with respect to the large eigenvalues provided that

$$D < D_N^{\text{large}} = \min_{k=1,...,N-1} D_{N,k}^{\text{large}}.$$

Proceeding as in §4.1 we find that the small eigenvalues are, up to a positive and $O(\varepsilon^2)$ multiplicative constant, equal to the eigenvalues of the matrix

$$\mathcal{H} = 2\omega\xi_c \nabla_{\boldsymbol{x}} \mathcal{G}_D \left(\mathcal{I}_N - 2\omega\xi_c \mathcal{G}_D\right)^{-1} \nabla_{\boldsymbol{x}} \mathcal{G}_D - \mathcal{Q}_D,$$

where $\mathcal{Q}_D$ is the $N \times N$ matrix with entries

$$(\mathcal{Q}_D)_{ij} = \begin{cases} \sum_{l \neq i} G''(x_i - x_l), & i = j, \\ -G''(x_i - x_j), & \text{otherwise.} \end{cases}$$

Since each of the matrices appearing in this expression are circulant they share the same eigenvectors and after substituting the common spike height ξ_c we obtain

$$\sigma_k(\mathcal{H}) = \frac{2\sigma_k(\nabla_{\boldsymbol{x}} \mathcal{G}_D)^2}{\sigma_0(\mathcal{G}_D) - 2\sigma_k(\mathcal{G}_D)} - \sigma_k(\mathcal{Q}_D).$$

As for the Schnakenberg case we note that $\sigma_0(\nabla_{\boldsymbol{x}} \mathcal{G}_D) = \sigma_0(\mathcal{Q}_D) = 0$ so that only the $k = 1, ..., N-1$ modes need to be considered. We likewise observe that for even N and $k = N/2$ the corresponding small eigenvalue is always linearly stable. Otherwise we find the small eigenvalue stability threshold $D_{N,k}^{\text{small}}$ by numerically solving

$$\frac{2\sigma_k(\nabla_{\boldsymbol{x}} \mathcal{G}_D)^2}{\sigma_0(\mathcal{G}_D) - 2\sigma_k(\mathcal{G}_D)} - \sigma_k(\mathcal{Q}_D) = 0.$$

Our numerical calculations again indicate that the small eigenvalue threshold for different modes differ as shown in Figure 6a. Interestingly, it appears that the mode with the minimum threshold value changes as s_2 is varied. We likewise numerically calculate the large eigenvalue thresholds and

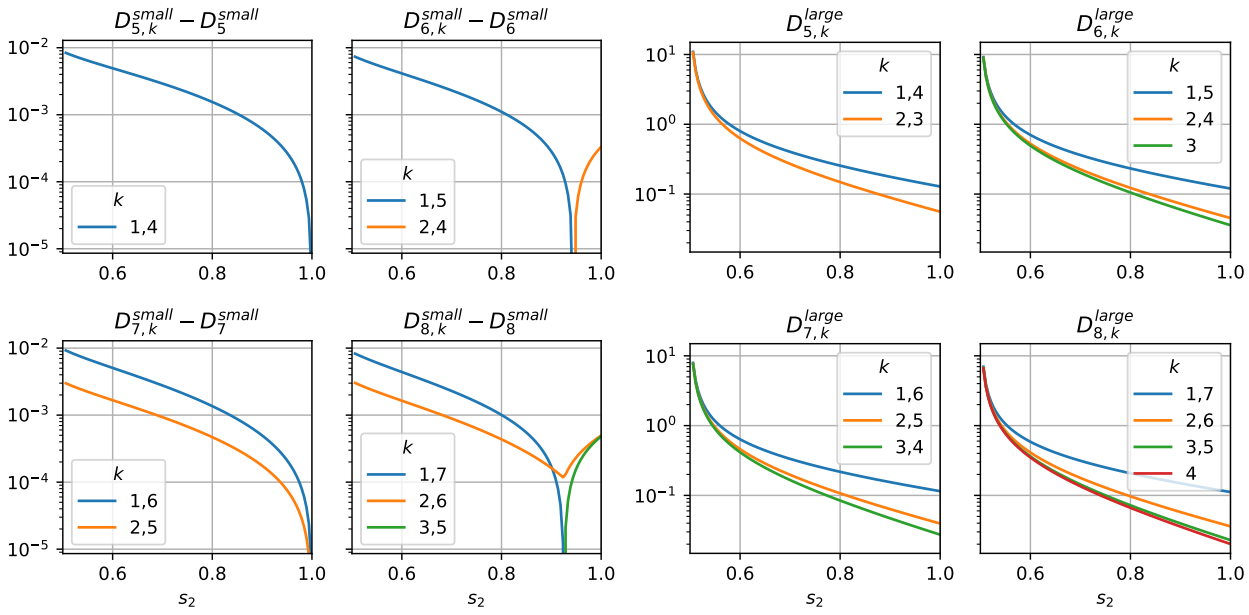

(A) (B)

FIGURE 6. Mode-dependent stability thresholds for the Gierer-Meinhardt system: (A) Small eigenvalue stability thresholds $D^{\text{small}}_{N,k}$. (B) Large eigenvalue stability thresholds $D^{\text{large}}_{N,k}$. Note that all plots share a common y-axis indicated by the left-most figure.

these are shown in Figure 6b. Next we minimize the thresholds $D^{\text{small}}_{N,k}$ and $D^{\text{large}}_{N,k}$ over all modes to obtain the small- and large-eigenvalue thresholds which we respectively denote by D^{small}_N and D^{large}_N. The results of these numerical calculations can be found in Figure 7a. We again observed from our numerical calculations that $D^{\text{large}}_N < D^{\text{small}}_N$ for even values of N and the inequality is reversed for odd N values (see Figures 7b and 7c). In summary, we observe that the linear stability thresholds for the subcritical Gierer-Meinhardt systems shares many similarities with the Schnakenberg system.

7. Numerical Simulations

To validate the numerically calculated stability thresholds from §3 and §4 we include here a brief outline of some numerical simulations of the full system (1.1). We use the numerical discretization and time-stepping algorithms used in [8, 17, 5] where we refer the reader for additional details. In short we use the finite-difference-quadrature methods in [10] to spatially discretize the fractional Laplacians in (1.1) and then perform time stepping with a second-order semi-implicit backwards difference scheme (SBDF-2) bootstrapped with a first-order semi-implicit backwards scheme (SBDF-1) [23].

We include here numerical simulations performed for $s_1 = 0.5$, $s_2 = 0.9$, $A = 0.01$, and $\varepsilon = 0.01$. We discretized the domain $-1 < x < 1$ with 1000 points and used a time step size of 0.0001 in the SBDF-2 scheme, using five steps of SBDF-1 with a step size of 0.00002 to get the two initial conditions required for SBDF-2. We observed good agreement with the asymptotically predicted stability thresholds. Mainly, the symmetric N spike solution was seen to be stable for values of D below the small (resp. large) eigenvalue threshold when N was odd (resp. even), and

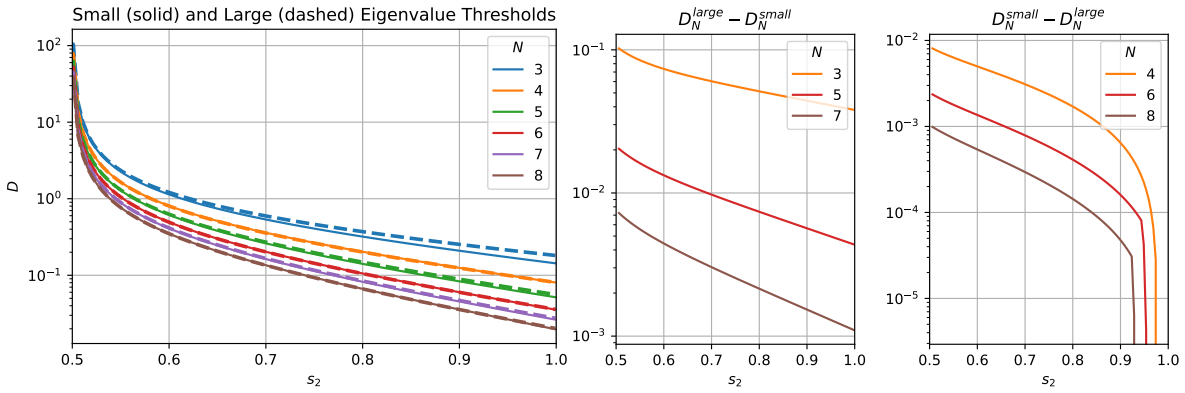

(A) (B) (C)

FIGURE 7. Numerical threshold calculations for the Gierer-Meinhardt system: (A) Small and large eigenvalue stability thresholds D_N^{small} and D_N^{large} versus s_2. (B) Difference between the large and small eigenvalue thresholds for odd N, and (C) difference between the small and large eigenvalue thresholds for even N.

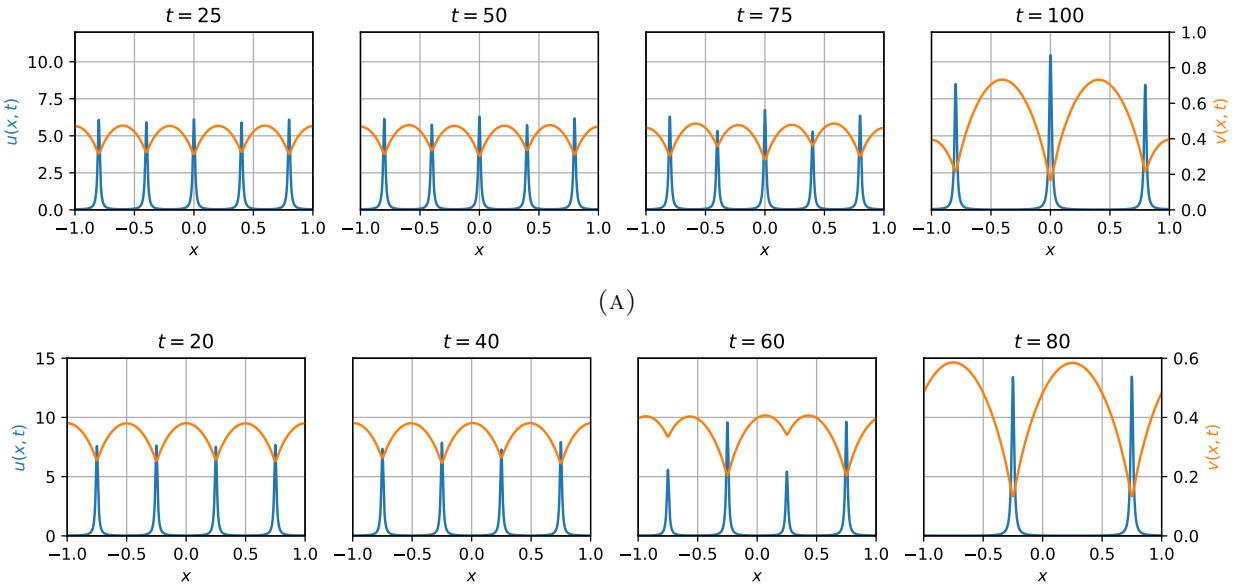

(A)

(B)

FIGURE 8. Plots of $u(x,t)$ (in blue with corresponding left axis) and $v(x,t)$ (in orange with corresponding right axis) obtained from a numerical simulation of (1.1). In (A) we use $D = 1.05D_5^{\text{small}}$ with the initial condition being a small perturbation from the asymptotically constructed symmetric 5-spike solution. In (B) we use $D = 1.05D_4^{\text{large}}$ with the initial condition being a small perturbation from the asymptotically constructed symmetric 4-spike solution.

unstable otherwise. In Figures 8a and 8b we respectively show the dynamics of a symmetric solution consisting of $N = 5$ and $N = 4$ spikes with $D = 1.05D_5^{\text{small}}$ and $D = 1.05D_4^{\text{large}}$.

8. Conclusions

In this paper we have used the method of matched asymptotic expansions to construct symmetric N-spike solutions to the singularly perturbed fractional Schnakenberg system. In addition we analysed the linear stability of these symmetric N-spike solutions with respect to both the large (or $O(1)$) and small (or $O(\varepsilon^2)$) eigenvalues. For the former, we derived in §3 a nonlocal eigenvalue problem (NLEP) from which the stability of the large eigenvalues could be determined by looking at the spectrum of some circulant matrices related to the Green's function satisfying (2.9). On the other hand, the linear stability with respect to the small eigenvalues was determined by deriving in §4 a system of ODEs for the slow-dynamics and then considering its linearization about the symmetric N-spike solution. This analysis yielded the interesting result that for $N \geq 5$ a symmetric N-spike solution will have distinct small-eigenvalue stability thresholds for different instability modes. This is in sharp contrast to the classical case for which the small eigenvalue thresholds are found to coincide. In §6 we verified that this behaviour also appears in the fractional Gierer-Meinhardt system, which suggests it may be a common feature for singularly perturbed fractional systems.

In addition to calculating stability thresholds we also performed in §5 a numerical continuation from symmetric N-spike solutions using the continuation software PyDSTool [2]. This continuation revealed that for $N = 5$ there are distinct asymmetric solution branches that bifurcate from different points along the symmetric N-spike solution branch. Although numerical simulations suggest that these asymmetric solutions are linearly unstable, a more comprehensive analysis of these solutions falls outside of the scope of this paper. Some interesting questions for future work in this direction is to determine whether the fractional order has any bearing on the linear stability of these asymmetric solutions and in particular whether they can be stabilized. Finally, we comment that the Green's function satisfying (2.9) and given by (2.11) was prominently featured throughout both the construction of equilibrium solutions and analysis of their linear stability. In Appendix A we calculated the regular part (A.3) with which the resulting expression (2.11) yields a rapidly converging series expansion. We believe that these quickly convergins series will be of use for further studies of singularly perturbed fractional systems with other reaction kinetics such as the Gray-Scott and Brusselator systems.

Acknowledgement

D. Gomez is supported by NSERC and the Simons Foundation, Z. Yang is partially supported by NSERC, and J. Wei is partially supported by NSERC.

Competing Interests

The authors don't have any financial or non-financial competing interests to disclose in relation to this paper.

References

[1] A. M. Alexander and S. D. Lawley. Reaction-subdiffusion equations with species-dependent movement. *SIAM Journal on Applied Mathematics*, 81(6):2457–2479, 2021.

[2] R. H. Clewley, W. Sherwood, M. LaMar, and J. Guckenheimer. Pydstool, a software environment for dynamical systems modeling. *URL http://pydstool. sourceforge. net*, 2007.

[3] N. Ehstand, C. Kuehn, and C. Soresina. Numerical continuation for fractional pdes: sharp teeth and bloated snakes. *Communications in Nonlinear Science and Numerical Simulation*, 98:105762, 2021.

[4] A. A. Golovin, B. J. Matkowsky, and V. A. Volpert. Turing pattern formation in the Brusselator model with superdiffusion. *SIAM J. Appl. Math.*, 69(1):251–272, 2008.

[5] D. Gomez, M. Medeiros, J. Wei, and W. Yang. Spike solutions to the supercritical fractional Gierer-Meinhardt system. *Article submitted for publication.*

[6] D. Gomez, M. J. Ward, and J. Wei. The linear stability of symmetric spike patterns for a bulk-membrane coupled Gierer-Meinhardt model. *SIAM J. Appl. Dyn. Syst.*, 18(2):729–768, 2019.

[7] D. Gomez, M. J. Ward, and J. Wei. An asymptotic analysis of localized three-dimensional spot patterns for the Gierer-Meinhardt model: Existence, linear stability, and slow dynamics. *SIAM Journal on Applied Mathematics*, 81(2):378–406, 2021.
[8] D. Gomez, J. Wei, and W. Yang. Stability of spike solutions to the fractional gierer-meinhardt system in a one-dimensional domain. *Numerical Mathematics: Theory, Methods and Applications*, 15(4):938–989, 2022.
[9] B. Henry, T. Langlands, and S. Wearne. Turing pattern formation in fractional activator-inhibitor systems. *Physical review. E, Statistical, nonlinear, and soft matter physics*, 72:026101, 09 2005.
[10] Y. Huang and A. Oberman. Numerical methods for the fractional laplacian: A finite difference-quadrature approach. *SIAM Journal on Numerical Analysis*, 52, 11 2013.
[11] D. Iron and M. J. Ward. The dynamics of multispike solutions to the one-dimensional Gierer-Meinhardt model. *SIAM J. Appl. Math.*, 62(6):1924–1951, 2002.
[12] D. Iron, M. J. Ward, and J. Wei. The stability of spike solutions to the one-dimensional Gierer-Meinhardt model. *Phys. D*, 150(1-2):25–62, 2001.
[13] H. K. Khudhair, Y. Zhang, and N. Fukawa. Pattern selection in the schnakenberg equations: From normal to anomalous diffusion. *Numerical Methods for Partial Differential Equations*, 2021.
[14] T. Kolokolnikov, M. J. Ward, and J. Wei. Spot self-replication and dynamics for the schnakenberg model in a two-dimensional domain. *J. Nonlinear Sci.*, 19(1):1–56, 2009.
[15] A. Lischke, G. Pang, M. Gulian, F. Song, C. Glusa, X. Zheng, Z. Mao, W. Cai, M. M. Meerschaert, M. Ainsworth, and G. E. Karniadakis. What is the fractional laplacian? a comparative review with new results. *Journal of Computational Physics*, 404:109009, 2020.
[16] B. A. Malomed. Optical solitons and vortices in fractional media: a mini-review of recent results. In *Photonics*, volume 8, page 353. MDPI, 2021.
[17] M. Medeiros, J. Wei, and W. Yang. Existence and stability of symmetric and asymmetric patterns for the half-laplacian Gierer-Meinhardt system in one-dimensional domain. *To appear in Math. Models Methods Appl. Sci.*
[18] R. Metzler and J. Klafter. The restaurant at the end of the random walk: recent developments in the description of anomalous transport by fractional dynamics. *Journal of Physics A: Mathematical and General*, 37(31):R161–R208, jul 2004.
[19] V. Minden and L. Ying. A simple solver for the fractional laplacian in multiple dimensions. *SIAM Journal on Scientific Computing*, 42(2):A878–A900, 2020.
[20] Y. Nec. Spike-type solutions to one dimensional Gierer–Meinhardt model with Lévy flights. *Studies in Applied Mathematics*, 129(3):272–299, 2012.
[21] Y. Nishiura. *Far-from-equilibrium dynamics*, volume 209 of *Translations of Mathematical Monographs*. American Mathematical Society, Providence, RI, 2002. Translated from the 1999 Japanese original by Kunimochi Sakamoto, Iwanami Series in Modern Mathematics.
[22] I. Rozada, S. J. Ruuth, and M. J. Ward. The stability of localized spot patterns for the Brusselator on the sphere. *SIAM J. Appl. Dyn. Syst.*, 13(1):564–627, 2014.
[23] S. J. Ruuth. Implicit-explicit methods for reaction-diffusion problems in pattern formation. *J. Math. Biol.*, 34(2):148–176, 1995.
[24] W. H. Tse, J. Wei, and M. Winter. The Gierer-Meinhardt system on a compact two-dimensional Riemannian manifold: interaction of Gaussian curvature and Green's function. *J. Math. Pures Appl. (9)*, 94(4):366–397, 2010.
[25] J. C. Tzou, S. Xie, T. Kolokolnikov, and M. J. Ward. The stability and slow dynamics of localized spot patterns for the 3-D Schnakenberg reaction-diffusion model. *SIAM J. Appl. Dyn. Syst.*, 16(1):294–336, 2017.
[26] M. J. Ward and J. Wei. Asymmetric spike patterns for the one-dimensional Gierer-Meinhardt model: equilibria and stability. *European J. Appl. Math.*, 13(3):283–320, 2002.
[27] M. J. Ward and J. Wei. The existence and stability of asymmetric spike patterns for the schnakenberg model. *Studies in Applied Mathematics*, 109(3):229–264, 2002.
[28] J. Wei. On the interior spike layer solutions to a singularly perturbed neumann problem. *Tohoku Math. J. (2)*, 50(2):159–178, 1998.
[29] J. Wei and M. Winter. *Mathematial aspects of pattern formation in biological systems*, volume 189. Applied Mathematical Sciences Series, Springer, 2014.
[30] J. Wei and W. Yang. Multi-bump ground states of the fractional Gierer-Meinhardt system on the real line. *J. Dynam. Differential Equations*, 31(1):385–417, 2019.
[31] L. Zhang and C. Tian. Turing pattern dynamics in an activator-inhibitor system with superdiffusion. *Physical Review E*, 90, 12 2014.

Appendix A. A Rapidly Converging Green's Function

In this appendix we summarize the computation of the rapidly converging series expansion for the Green's function appearing in (2.11). We follow closely the methods used in [30, 8] by adding

and subtracting singular terms from the series expansion and refer to those references for further details. First we make note of the Fourier series

$$|x|^2 = \frac{1}{3} + 4\sum_{n=1}^{\infty} \frac{(-1)^n}{(\pi n)^2}\cos(\pi n x),$$

and

$$|x|^4 = -\frac{7}{15} + 2|x|^2 - 48\sum_{n=1}^{\infty} \frac{(-1)^n}{(\pi n)^4}\cos(\pi n x).$$

After repeatedly integrating by parts we then obtain the Fourier series

$$\begin{aligned} |x|^{\beta-1} =& \frac{1}{\beta} + 2(\beta-1)\Gamma(\beta-1)\cos\left(\frac{\pi\beta}{2}\right)\sum_{n=1}^{\infty}\frac{\cos\pi n x}{(\pi n)^\beta} + \frac{\beta-1}{2}\left(|x|^2 - \frac{1}{3}\right) \\ &- \frac{(\beta-1)(\beta-2)(\beta-3)}{24}\left(2|x|^2 - |x|^4 - \frac{7}{15}\right) \\ &+ 2(\beta-1)\cdots(\beta-5)\sum_{n=1}^{\infty}\frac{a_{\beta,n}}{(\pi n)^\beta}\cos(\pi n x), \end{aligned} \tag{A.1}$$

where

$$a_{\beta,n} = \int_{\pi n}^{\infty} x^{\beta-6}\sin x dx. \tag{A.2}$$

Substituting $\beta = 2s_2$ we thus obtain (2.11) where

$$\begin{aligned} R(x) = \mathfrak{a}_{s_2}\Bigg[&\frac{1}{2s_2} - \frac{2s_2-1}{6} + \frac{7}{15}\frac{(2s_2-1)(2s_2-2)(2s_2-3)}{24} \\ &+ \left(\frac{2s_2-1}{2} - \frac{(2s_2-1)(2s_2-2)(2s_2-3)}{12}\right)|x|^2 \\ &+ \frac{(2s_2-1)(2s_2-2)(2s_2-3)}{24}|x|^4 \\ &+ 2(2s_2-1)\cdots(2s_2-5)\sum_{n=1}^{\infty}\frac{a_{2s_2,n}}{(\pi n)^{2s_2}}\cos(\pi n x)\Bigg]. \end{aligned} \tag{A.3}$$

Appendix B. Eigenvalues of Circulant Matrices

The symmetric N-spike configurations with points arranged according to (2.17a) results in several *circulant* matrices throughout the paper. An $N \times N$ circulant matrix B has the general form

$$B = \begin{pmatrix} b_0 & b_1 & b_2 & \cdots & b_{N-1} \\ b_{N-1} & b_0 & b_1 & \cdots & b_{N-2} \\ \vdots & \vdots & \vdots & \ddots & \vdots \\ b_1 & b_2 & b_3 & \cdots & b_0 \end{pmatrix}. \tag{B.1}$$

The eigenvectors of such a matrix are given by

$$\boldsymbol{v}_k = \left(1, e^{i\frac{2\pi k}{N}}, e^{i\frac{4\pi k}{N}}, e^{i\frac{6\pi k}{N}}, \cdots, e^{i\frac{2(N-1)\pi k}{N}}\right)^T, \qquad k = 0, ..., N-1, \tag{B.2}$$

which we remark are independent of the entries $b_0, ..., b_{N-1}$. Therefore all circulant matrices share the same eigenvectors. Moreover the eigenvalues are given by

$$\sigma_k(B) = \sum_{j=0}^{N-1} b_j e^{i\frac{2\pi jk}{N}}, \qquad k = 0, ..., N-1. \tag{B.3}$$

If in addition to being circulant the matrix B is also symmetric, then the eigenvalues are real valued and given by

$$\sigma_k(B) = \sum_{j=0}^{N-1} b_j \cos\left(2\pi jk/N\right) = \begin{cases} b_0 + 2\sum_{j=1}^{N/2} b_j \cos\left(2\pi jk/N\right), & \text{if } N \text{ is even,} \\ b_0 + 2\sum_{j=1}^{(N-1)/2} b_j \cos\left(2\pi jk/N\right), & \text{if } N \text{ is odd,} \end{cases} \tag{B.4}$$

whereas if is skew-symmetric, then the eigenvalues are imaginary and given by

$$\sigma_k(B) = i\sum_{j=1}^{N-1} b_j \sin\left(2\pi jk/N\right) = \begin{cases} 2i\sum_{j=1}^{N/2-1} b_j \sin\left(2\pi jk/N\right), & \text{if } N \text{ is even,} \\ 2i\sum_{j=1}^{(N-1)/2} b_j \sin\left(2\pi jk/N\right), & \text{if } N \text{ is odd,} \end{cases} \tag{B.5}$$

for each $k = 0, ..., N-1$. Note that when N is even and B is skew symmetric we have $\sigma_{N/2}(B) = 0$.

Daniel Gomez, Department of Mathematics, University of Pennsylvania, Philadelphia, PA USA 19104-6395

Email address: d1gomez@sas.upenn.edu

Jun-cheng Wei, Department of Mathematics, The University of British Columbia, Vancouver, BC Canada V6T 1Z2

Email address: jcwei@math.ubc.ca

Zhangyu, Department of Mathematics, The University of British Columbia, Vancouver, BC Canada V6T 1Z2

Email address: yzy735@student.ubc.ca